DOI: 10.24996/ijs.2025.66.4.2

ISSN: 0067-2904

Determination of Cobalt(II) Ion in Various Selected Alloys *via* Utilizing Continous Flow Injection Analysis ((CFIA) (Nagham-Four Sources of White Snow LED Arranged in Three Rows Corresponding to Three Detectors Analyzer) (NAG-4SX3-3D)) Analyzer at 0-180º Angle

Bakr Sadiq*, Nagham Shaker

College of Science, Chemistry Department, University of Baghdad, Baghdad, Iraq.

Received: 16/6/2023 Accepted: 12/5/2024 Published: 30/4/2025

Abstract

The research study focuses on the efficient and accurate detection and determination of cobalt ions. The detection method involves the formation of brilliant green aggregates with calcium hexacyanoferrate in the presence of nitric acid. (Nagham-four sources of white snow light-emitting diodes arranged in three rows corresponding to three detectors) (The NAG-4SX3-3D Analyzer is an optical, chemical, electronic, and detection tool that receives a cumulative signal (no amplification is required). The total distance travelled is 760 mm with regard to YZ(mV) - tsec (dmm). It was selected for its precise calculation of the energy transducer profile. The linear range for measuring cobalt (II) ions is 0.05 to 20 mM. For concentrations of 5 and 10 mM, the relative standard deviation (RSD) for eight repeated intraday measurements is less than 0.36%. The calibration graph gradually dilutes the lowest concentration to determine the limit of detection (LOD) of 349.236 ng per analyte sample. The correlation coefficient (r) for the linear dynamic range is 0.9893, and the linearity is 97.80% (R^2 %). The results of the proposed method were compared to the already-available UV-spectrophotometric technique at a wavelength of 510 nm and found to be comparable..

Keywords: Cobalt (II) ion, Continous flow injection analysis CFIA,NAG-4SX3-3D analyzer

تقدير أيون الكوبالت(II) في سبائك مختلفة عن طريق أستخدام محلل الحقن الجرياني المستمر(نغم-أربعة مصادر من الثلج الأبيض الثنائيات الباعثة للضوء مرتبة في ثلاثة صفوف تقابل ثلاثة كواشف NAG-4SX3-3Dعند زاوية 0-180°

بكر صادق* ، نغم شاكر

الكيمياء, كلية العلوم , جامعة بغداد, بغداد, العراق

الخلاصة

تركزت الدراسة على الكشف الفعال والدقيق عن أيونات الكوبلت الثنائية (II). تضمنت طريقة الكشف عن تكوين كتل خضراء لامعة مع سداسي سيانيد الحديديك الكالسيوم بوجود حامض النتريك . (نغم-أربعة مصادر من الضوء الأبيض الثلجي الثنائيات الباعثة للضوء مرتبة في ثلاثة صفوف تقابل ثلاثة كواشف)

---

*Email: bakralalazaw98@gmail.com

((NAG−4SX3−3D Analyzer) أداة كشف بصرية كيميائية إلكترونية تعتمد على استقبال الإشارة التراكمية (لا تحتاج الى تضخيم) . يبلغ إجمالي مسافة السفر 760 مم فيما يتعلق بـ d) YZ(mV) – t sec (mm). تم اختيار المحلل NAG−4SX3−3D لحسابه الدقيق لاستجابة محلل الطاقة . المدى الخطي لقياس أيونات الكوبلت الثنائي (II) هو 0.05 إلى 20 ملي مولار. الانحراف المعياري النسبي (RSD) لتكرار ثمان مرات (ضمن اليوم) أقل من 0.36٪ لتراكيز 5 و 10 ملي مولار. أقل تركيز في منحنى المعايرة خفف لتحديد حد الكشف LOD) 349.236 نانوغرام لكل انموذج محلل. معامل الارتباط (r) للمدى الديناميكي الخطي هو 0.9893 ونسبة الخطية :(R^2 % 97.80). تمت مقارنة نتائج الطريقة المقترحة مع المتوفرة حاليا لتقنية القياس الطيفي الضوئي بالأشعة فوق البنفسجية بطول موجة 510 نانومتر ، ووجد أنها قابلة للمقارنة.

الكلمات المفتاحية: ايون الكوبلت الثنائي ، تحليل حقن الجرياني المستمر، محلل NAG−4SX3−3D.

1. Introduction

Cobalt is an important component of vitamin B12 and plays a significant role in the body. Therefore, monitoring the levels of cobalt in bodily fluids is crucial for managing vitamin B12 deficiency and potentially preventing its detrimental effects on appearance[1]. Despite cobalt's relatively low toxicity, its acute and persistent exposure can result in symptoms such as pulmonary oedema, nausea, hypersensitivity, gastrointestinal disorders, diarrhea, and other related ailments [2]. The genotoxic and carcinogenic properties of cobalt (II) particles are significant [3]. In the fields of natural science, nutrition, pollution control, toxicity, and hygiene, this metal particle is among the most notable of the hazardous metals [4]. Cobalt (II) particles have also been used in the development of sensing and integrated circuits [5-7]. Cobalt typically exists in the II oxidation state. Certain compounds rapidly convert cobalt (III). It is responsible for the formation of compounds involving amine, cyanide, tartrate, and EDTA [8]. Flow injection analysis method has been used in determination many componds[9-11] .A number of chemical techniques have been described that use light-emitting diodes (LEDs) as sources of incident light, many of which rely on continuous flow injection analysis , NAG-ADF-300-2 [12], For the measurement of cobalt (II) ions, many methods have been reported, such as X-ray photoelectron spectroscopy (XPS) [13, 14], Inductive Coupled Plasma-Flow Injection Analysis (ICP-FIA) [15, 16], Flame Atomic Absorption spectroscopy (FAAS) [17], Flow Injection Analysis FIA-Spectro [18], Continuous Flow Injection Analysis-Chemiluminometric CFIA-CL[19],and CFIA-CL Fluorescence (CFIA-CLF) [20-22]. The research presented here presents the first report on the utilization of the newly developed (Nagham-four sources of white snow LED arranged in three rows corresponding to three detectors (NAG-4SX3-3D Analyzer), which are based on flow analysis principles, for the optoelectronic determination of cobalt in turbidimetric samples. This research aims to estimate the cobalt ion, a crucial element in our lives, offering a fresh approach to the previously described traditional methods. Hence, a cost-effective and compact optoelectronic detector will be developed to enable comprehensive turbidimetric measurements in continuous flow injection analysis. In this investigation, a brilliant green precipitate product could be obtained utilizing the continuous flow injection analysis approach and measured by the precipitation of cobalt (II) ions by calcium hexacyanoferrate (II). The precipitate product will be determined at 0-180° using a homemade (NAG-4SX3-3D Analyzer).

2. Experiments

2.1. Materials

All of the reagents and chemicals utilized during this research were of analytical grade, unless stated otherwise. Table 1 presents the fundamental compounds that were used as standard stock solutions in the present investigation. Additional standard solutions were prepared through the process of diluting the original stock solution.

Table 1: A list of the essential chemicals and reagents utilized in this study

Name Concentration	**Formula details of stock solution**	**Company supplier**	**M.Wt. (g/mol)**	**Weight / volume or Volume / volume**	**Remarks**	**Reference**
Acetic acid *[0.5 mol.L^{-1}] **[0.425 mol.L^{-1}]	CH_3COOH 99.8%wt/wt Sp.gr.1.05g/mL	BDH	60.05	7.2 mL/250mL	Standardized with Na_2CO_3 solution	**[23]**
Ammonium acetate [0.25 mol.L^{-1}]	CH_3COONH_4	Fluka	77.08	1.927 g/100mL	Dissolved in distilled water	
Ammonium chloride [0.25 mol.L^{-1}]	NH_4Cl	Fluka	53.49	1.3373g/100mL	Dissolved in distilled water	
Calcium hexacyanoferrate [0.05 mol.L^{-1}]	$Ca_2[Fe(CN)_6].11\ H_2O$	Fluka	490.27	2.45135g/100mL	Dissolved in distilled water	
Hydrochloric acid *[0.5 mol.L^{-1}] **[0.463 mol.L^{-1}]	HCl -35%wt/wt Sp.gr.1.16g/mL	BDH	36.46	11.23 mL/250mL	Standardized with Na_2CO_3 solution	
Nitric acid *[0.5 mol.L^{-1}] **[0.431 mol.L^{-1}]	HNO_3 -70%wt/wt Sp.gr.1.42g/mL	BDH	63.01	7.92 mL/250mL	Standardized with Na_2CO_3 solution	
Phosphoric acid *[0.5 mol.L^{-1}] **[0.433 mol.L^{-1}]	H_3PO_4 85%wt/wt Sp.gr.1.84g/mL	BDH	97.994	12.76mL/250mL	Standardized with Na_2CO_3 solution	
Potassium chloride [0.25 mol.L^{-1}]	KCl	BDH	74.55	1.8638g/100mL	Dissolved in distilled water	
Potassium Iodide [0.25 mol.L^{-1}]	KI	BDH	166.00	4.15g/100mL	Dissolved in distilled water	
Sodium carbonate [0.25 mol.L^{-1}]	Na_2CO_3	BDH	105.99	2.6498g/100mL	Dissolved in distilled water	
Sodium chloride [0.25 mol.L^{-1}]	NaCl	BDH	58.44	1.461g/100mL	Dissolved in distilled water	
Sodium sulfate [0.25 mol.L^{-1}]	Na_2SO_4	BDH	142.04	3.551g/100mL	Dissolved in distilled water	
Sodium sulfite [0.25 mol.L^{-1}]	Na_2SO3	BDH	126..043	3.15g/100mL	Dissolved in distilled water	
Sulfuric acid *[0.5 mol.L^{-1}] **[0.43 mol.L^{-1}]	H_2SO_4 -96%wt/wt Sp.gr.1.84g/mL	BDH	98.08	7ml/250mL	Standardized with Na_2CO_3 solution	

*The chemical compound's initial concentration before being standardized using sodium carbonate solution.
** The chemical compound's final concentration after being standardized using sodium carbonate solution.

2.2. Apparatus

The signal that results from entering light being attenuated (0-180°) is acquired utilizing the flow chamber manufactured from a home-built NAG-4SX3-3D analyzer. It is composed of a metal jacket with two faces measuring 40 mm × 40 mm, one of which is used to enclose the irradiation sources in three rows, and each will be able to enclose four sources of W.S.LED (lined up). While the opposite side, which is at 0-180°, will be used to enclose the detector cells, which are three [23], as shown in Figure 1A. The output signals were recorded using potentiometric recorders in item number (Siemens, Germany). An ismatic peristaltic pump with six ports connects to a Teflon, variable-length sample loop. With the use of a UV spectrophotometric device (Shimadzu, Japan), the customary procedures were performed.

2.3. Methodology

The cobalt (II) ion reaction with calcium hexacyanoferrate (II) to produce a brilliant green precipitate was studied using a flow injection manifold system and a home-made NAG-4SX3-3D (NAG) instrument. It is composed of a metal jacket with two faces measuring 40 mm x 40 mm, by 40 mm. The first face encloses the irradiation sources in three rows, each of which can contain four W.S.LED sources arranged in a line-up configuration. The opposite side, which is at 0-180°, will be used to enclose the detector cells, which are three. The other four remaining sides are 40 mm × 50 mm. Drilling on one side results in three parallel holes, each with an outside diameter of 4 mm, extending to 40 mm, and passing through three transparent Pyrex glass tubes. Each tube is 60 mm in length and has an outside diameter of 4 mm. Teflon tubes, each measuring 300 mm in length and with an inside diameter of 1 mm, join the three tubes together. The brilliant green precipitate reaction was used as a new method for determining Co^{+2} with the NAG-4SX3-3D Analyzer-CFIA, which is shown in Figure 1A. In the experiment, the sample size was 60 µL, there was 10 mM of Co^{+2}, 2 mM of $Ca_2[Fe(CN)_6]$, and the flow rate for both the transporter stream (H_2O) and the agent stream ($Ca_2[Fe(CN)_6]$) was 1.8 $mL.min^{-1}$. The transporter stream line (H_2O) transferring the sample of Co^{+2} (10 mM) *via* the six-port injection valve. is illustrated in Figure 1A, in which the Y-junction point meets and mixes both the carrier stream line and the reagent line together and leads to the formation of brilliant green precipitate particulate, which in turn grows and agglomerates during their flow to the NAG. The response profile (Yzi (mV) versus. t_{min} (d_{mm})) was recorded using a potentiometric recorder to measure transmitted height at (0-180°), which was expressed in mV as a peak light, as shown in Figure 1B. Scheme 1 illustrates the proposed reaction between Co^{+2} and $Ca_2[Fe(CN)_6]$ in the aqueous medium [24].

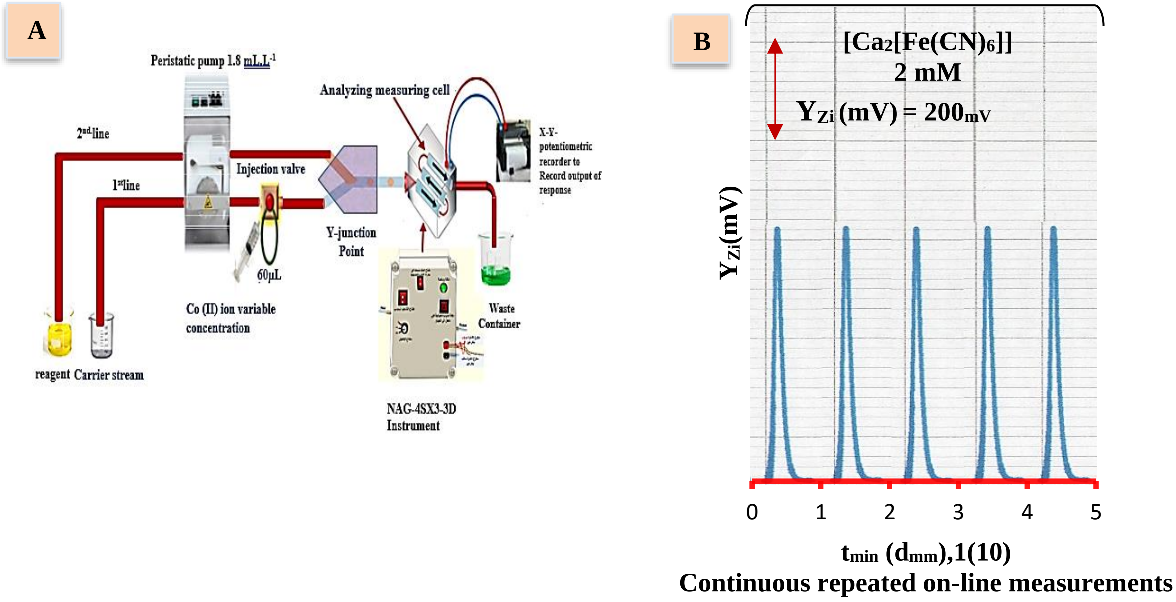

Figure 1A: flow gram manifold system for quantification of Co^{+2} using Co (II)- $[Fe(CN)_6]^{4-}$ system **1B**: Profile of Y_{zi} (mV) versus time (distance) 1(10) of 60µL of Co^{+2} and 60 cm/min speed of recorder

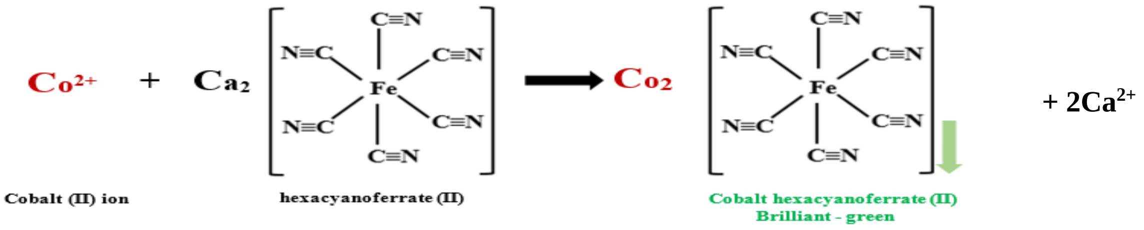

Scheme 1: Proposed reaction using Co^{+2} - $[Fe(CN)_6]^{-4}$ system to form brilliant - green precipitate particulate

3. Results and discussion

The flow injection manifold system shown in Figure 1A was used to look at chemical and physical parameters in order to find the conditions that would make the white precipitate reaction product with the highest level of repeatability and sensitivity. Keeping them all constant while making changes to them one at a time was the most effective strategy to optimize these variables.

3.1. Chemical parameters

3.2. Effect of variable concentration of Ca_2 [Fe $(CN)_6$]

The sample volume was 60 µL, and the Co^{+2} concentration was kept constant at 10 mM. It can be seen that an increase in $Ca_2[Fe(CN)_6]$ leads to the prevention of part of incident light, causing an increase in the attenuation of light and an increase in the peak height due to an increase in the formation of solid particulate in different forms, crystalline or colloidal precipitated reaction product up to 5 mM, followed by a decrease in peak height at a concentration higher than 5 mM, as shown in Figure 2A. Therefore, 5 mM of Ca_2 $[Fe(CN)_6]$ concentration was regarded as the optimum concentration used for further work (Table 2A). Also the slope-intercept method (Figure 2B) supports this choice as the segment no.2 (a_4-a_6) in the range of 5-10 mM has the largest intercept and the lowest slope, ϴ value, and r, respectively, whereas the other segments have a low sensitivity. Table 2B demonstrates that the optimal section was S_2 (5-10 mM), with 5 mM being the selected segment.

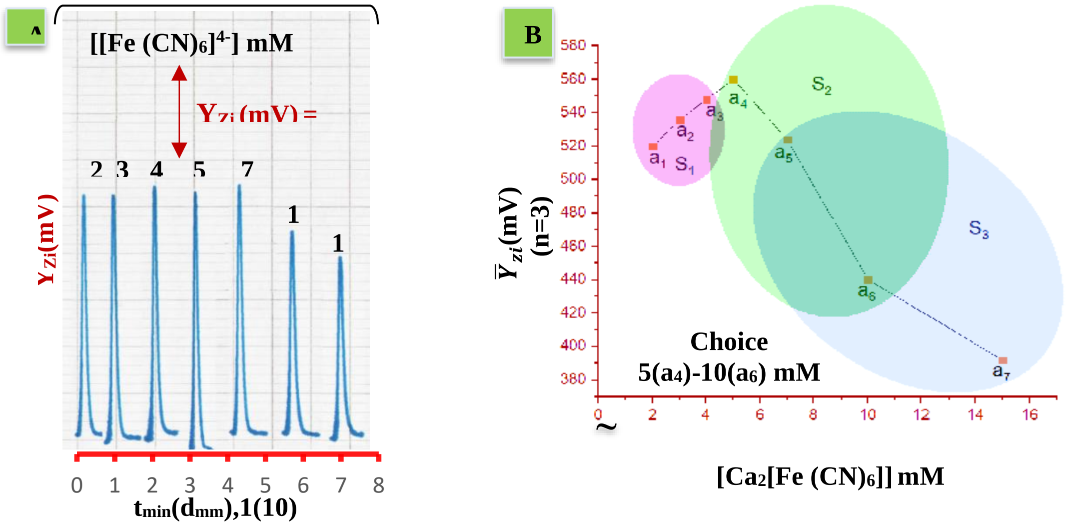

Figure 2: A: Effect of calcium hexacyanoferrate (II) concentrations on the response profile. **B:** $\bar{Y}_{Z\,i}$ (mV) output of the signal-to-noise ratio (S/N) response of the finest choice together with an energy detector and three points of data blended into a single segment

Table 2A: The influence of the calcium hexacyanoferrate concentration (II) on the precipitation of Co^{+2}.
2B: Choosing the best segment in accordance with the requirements of the segment pattern, for Co^{+2}-(calcium hexacyanoferrate) reaction system

A			
[reagent] mM	**$\bar{Y}_{Zi}$(mV) average (n=3)**	**%RSD σ_{n-1}(n:3)**	**CI at 0.05 $\bar{Y}_{Zi} \pm t * \sigma_{n-1}/\sqrt{3}$**
2	520	0.24	520±3.056
3	536	0.41	536±5.490
4	548	0.26	548±3.304
5	560	0.24	560±3.006
7	524	0.48	524±6.260
10	440	0.60	440±6.508
15	392	0.59	392±5.738

B					
Segment	**[reagent] range mM**	**Intercept(a)mV**	**Slope(b) mV/ mM**	**Correlation Coefficient(r)**	**Angle Ɵ**
$S_1(a_1\text{-}a_3)$	2-4	492.66	14.0	0.9966	85.914
$S_2(a_4\text{-}a_6)$	5-10	686.32	-24.32	-0.9937	-87.645
$S_3(a_5\text{-}a_7)$	7-15	620.49	-15.79	-0.955	-86.377
$\bar{Y}_{Zi}$(mV):(S/N response of NAG-4SX3-3D Analyzer) in mV((S/N)-R.N.A), $t_{0.025,2}$=4.303, SEM= Standard error of mean.					

3.3. Effect of reaction medium (selected salts and acids)

In addition to aqueous medium, i.e., distilled water, with a sample volume of 60 microliters at a flow rate of 1.8 mL.min^{-1} for each line of the two-line system, the reaction of Co^{+2} (10 mM) and $[Fe(CN)_6]^{-4}$ (5 mM) has been studied in different media, including acids and salts (100 mM) (Table 1). Figure 3 displays the profiles of responses. While Table 3 lists all the findings, The reactions are decreased by all used salts; this might be due to the peptization process during the precipitation process or a dissolution of solid particles that results in a decrease or reduction in the dense mass of precipitate. Even when compared to distilled water (D.W.) and other acids. The nitric acid solution responded more clearly, exhibiting a high response rate. The ions may have helped make a thick precipitate and lowered the intermolecular gups, which led to granulation and the growth of compact crystals that will act as a reflective surface. Researchers discovered that nitric acid solution, instead of several salts, acids, and deionized water, was the most suitable transporter stream for maximal incoming light attenuation.

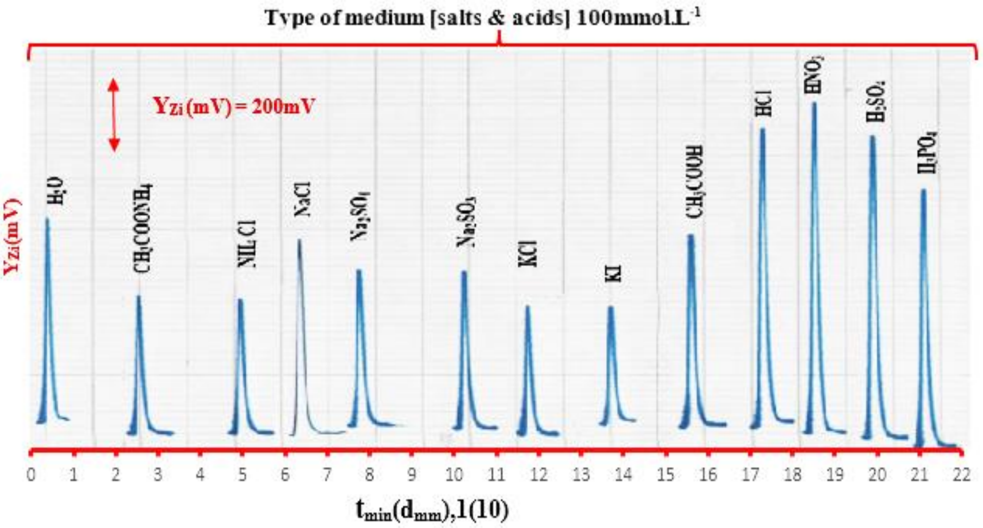

Figure 3: Acids and salts' effects on the response profile

Table 3: Effect of various media on the precipitation of the Co^{+2} (10 mM)-$[Fe(CN)_6]^{-4}$ (5 mM) system

Type of medium	$\bar{Y}_{Zi}$(mV) average (n=3)	RSD% σ_{n-1}(n:3)	CI at 0.05 $\bar{Y}_{Zi} \pm t * \sigma_{n-1}/\sqrt{3}$
[Salt] = 100mM			
H_2O	560	0.22	560±3.006
CH_3COONH_4	384	0.56	384±5.291
NH_4Cl	376	0.62	376±5.788
NaCl	536	0.43	536±5.813
Na_2SO_4	432	0.74	432±7.974
Na_2SO_3	432	0.42	432±4.521
KCl	360	0.68	360±6.161
KI	328	0.71	328±5.763
$[H3O^+]$ = 100mM			
H_2O	560	0.22	560±3.006
CH3COOH	528	0.25	528±3.3538
HCl	824	0.23	824±4.7699
HNO_3	908	0.13	908±3.055
H_2SO_4	832	0.19	832±3.925
H_3PO_4	704	0.24	704±4.273
$\bar{Y}_{Zi}$(mV):(S/N response of NAG-4SX3-3D Analyzer) in mV((S/N)-R.N.A), $t_{0.025,2}$=4.303, SEM= Standard error of mean			

3.4. Nitric acid concentration

Co^{+2} (10 mM)-$Ca_2[Fe(CN)_6]$ (5 mM)-HNO_3 system. Depending on the concentration, we produced and used between 50 and 400 mM of nitric acid as the carry line spray. A flow rate of 1.8 mL.min^{-1}. It served as a transport stream, with the agent 60 µL serving as the sample volume. It was conducted with three consecutive measurements for each sample. Figure 4 shows that as the concentration of HNO_3 rises, the production of small-sized particulates, particularly those shaped like a nucleus and capable of collecting additional particles, further attenuates entering light. Its tightly packed, walled structure will aid in agglomeration, boosting incident light attenuation. A rise in the solubility of tiny particles is caused by concentrations greater than 150 mM. So, for the Co(II) ion (10 mM) - $Ca_2[Fe(CN)_6]$ (5 mM) - HNO_3 system, 150 mM of HNO_3 has been selected as the best transport stream, and Table 4A tallied the results. Findings demonstrating the calculation of the angle, correlation coefficient slope, and intercept, and Table 4B indicate that segment S_3 is the optimum (i.e., the portion includes 150 mM).

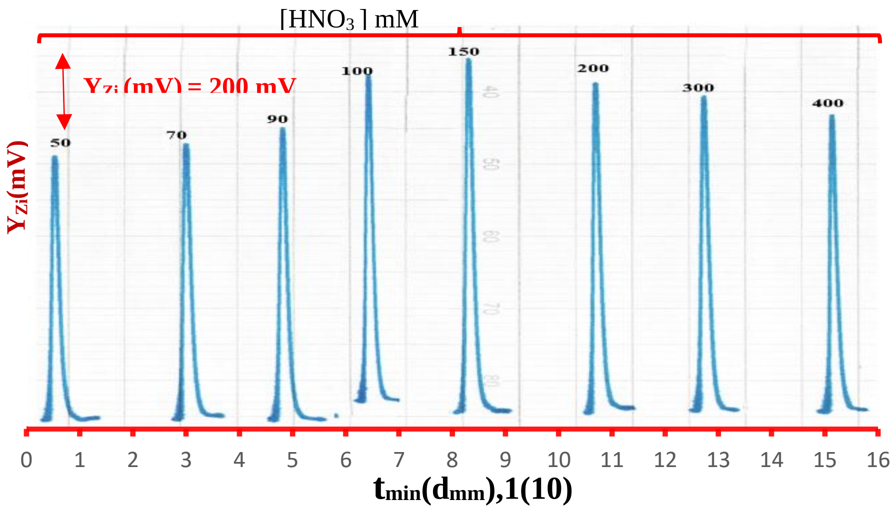

Figure 4: Response profile for the variation of nitric acid on Co^{+2} precipitation

Table 4A: The effect of various [nitric acid] concentrations on Co^{+2} precipitation
4B: Using a segmentation pattern, the Co^{+2} (10 mM)-$[Fe(CN)_6]^{-4}$ (5 mM)-HNO_3 system's best segment was chosen

A			
$[HNO_3]$mM	$\bar{Y}_{Zi}$(mV) average (n=3)	%RSD σ_{n-1}(n:3)	CI at 0.05 $\bar{Y}_{Zi}(mV) \pm t * \sigma_{n-1}/\sqrt{3}$
50	736	0.24	736±4.4220
70	768	0.25	768±4.7947
90	816	0.22	816±4.546
100	908	0.19	908±4.372
150	980	0.19	980±4.670
200	920	0.25	920±5.7636
300	880	0.24	880±5.291
400	824	0.25	824±5.2419

B					
Segment	$[HNO_3]$ mM	Intercept(a) mV	Slope(b) mV/ mM	correlation coefficient(r)	Angle ϴ
$S_1(a_1-a_3)$	50-90	633.33	2.00	0.993	63.434
$S_2(a_3-a_5)$	90-150	638.84	2.32	0.906	66.647
$S_3(a_5-a_8)$	150-300	1062.86	-0.63	-0.954	-32.152
$S_4(a_6-a_8)$	200-400	1018.66	-0.48	-0.995	-25.641

$\bar{Y}_{Zi}$(mV):(S/N response of NAG-4SX3-3D Analyzer) in mV((S/N)-R.N.A), $t_{0.025,2}$=4.303, SEM= Standard error of mean

3.5. Physical variables

3.5.1. Flow rate

Applying Co^{+2} (10mM) utilizing the$[Fe(CN)^6]^{-4}$ (5 mM) nitric acid (150 mM) is the system used with varied flow rates (F.R.) ranging from 0.9 to 2.8 $mL.min^{-1}$ for the carry line stream and agent. Both lines used a sample volume of 60 μL for both lines. Fig. 5A demonstrates how, at slow flow rates, a large particulate with a large volume, regarded as a heavy particulate, will not cope with the movement of the carrier stream through flow, causing a delay and elongation in the measuring cell, which causes a deformed profile with a wide (Δt_B). The NAG-4SX3-3D analyzer's (S/N) energy transducer output responses increased when the flow rate was increased to 1.6 $mL.min^{-1}$. The lack of sufficient time for the crystals to grow to a larger particle size that will enhance the attenuation of incoming light is most likely what causes a drop in peak heights at more than 1.6 $mL.min^{-1}$. To get the maximal response, 1.6 $mL.min^{-1}$ was used as the flow rate for both the carry line and agent streams. Figure 5B shows the F.R. change compared to the response curve of the (NAG) analyzer's S/N energy transducer output. The outcomes were listed in Tables 5A and 5B. Using the table's intercept, slope, correlation coefficient, and angle values, Segment S_2 (1.3-1.6 mL.min^{-1}) was shown to be the most effective one using Figures 5A and 5B, with 1.6 mL.min^{-1} serving as the appropriate (F.R.) carry line and agent utilized in the following trials.

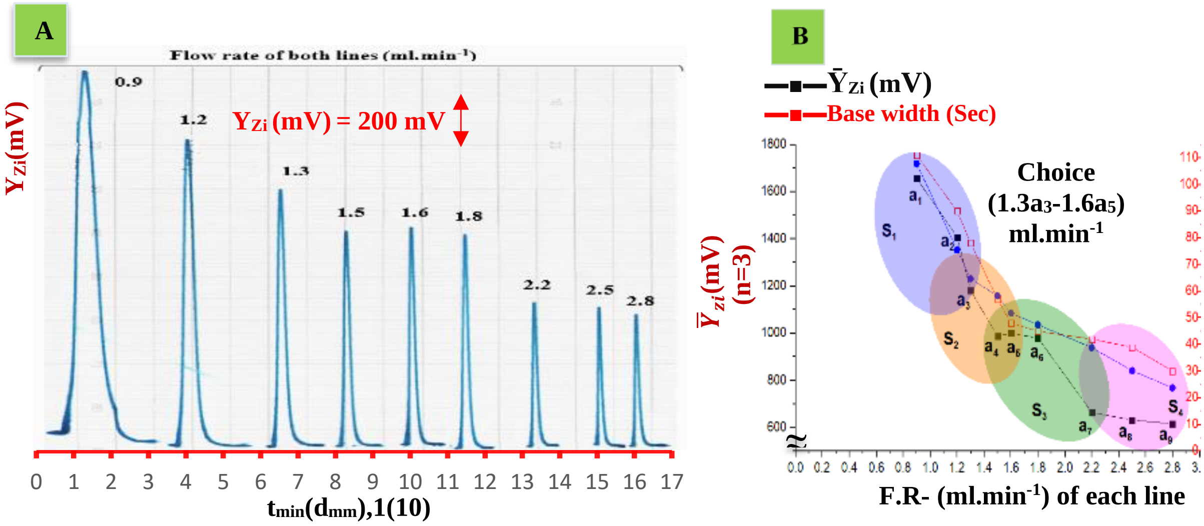

Figure 5A: Response graph for the evaluation's effect of flow rate on energy detector outputs of the NAG-4SX3-3D Analyzer through the production of the brilliant-green portion. **5B**: $\bar{Y}_{Z\,i}$ (mV) (S/N) RNA and three data points combined into one segment, with the best possible option

Table 5A: flow rate variation's impact on Co^{+2} precipitation. **5B**: Using a segmentation pattern, the Co^{+2} (10 mM)-[Fe (CN)$_6$]$^{-4}$ (5 mM)-HN0$_3$(150 mM) system's, at 60 µL sample volume, and the best segment was chosen

<table>
<tr><th colspan="10">A</th></tr>
<tr><th>Peristaltic speed</th><th>F.R mL/min of two line</th><th>$\bar{Y}_{Zi}$(mV) (n:3)</th><th>%RSD σ_{n-1}(n;3)</th><th>CI at 0.05 $\bar{Y}_{Zi}$(mV)± t*$\sigma_{n-1}/\sqrt{3}$</th><th>Δt_{B}Sec</th><th>V(mL) add</th><th>C (mM)</th><th>D.F</th><th>t_{sec}</th></tr>
<tr><td>5</td><td>0.9</td><td>1656</td><td>0.07</td><td>1656±3.006</td><td>111</td><td>3.39</td><td>0.177</td><td>56.497</td><td>30.0</td></tr>
<tr><td>10</td><td>1.2</td><td>1408</td><td>0.10</td><td>1408±3.528</td><td>90</td><td>3.66</td><td>0.164</td><td>60.976</td><td>21.0</td></tr>
<tr><td>15</td><td>1.3</td><td>1180</td><td>0.13</td><td>1180±3.925</td><td>78</td><td>3.44</td><td>0.174</td><td>57.471</td><td>18.0</td></tr>
<tr><td>20</td><td>1.5</td><td>988</td><td>0.14</td><td>988±3.577</td><td>57</td><td>2.91</td><td>0.206</td><td>48.544</td><td>16.2</td></tr>
<tr><td>22</td><td>1.6</td><td>1000</td><td>0.15</td><td>1000±3.925</td><td>48</td><td>2.62</td><td>0.229</td><td>43.667</td><td>14.4</td></tr>
<tr><td>25</td><td>1.8</td><td>980</td><td>0.13</td><td>980±3.329</td><td>45</td><td>2.76</td><td>0.217</td><td>46.083</td><td>13.2</td></tr>
<tr><td>30</td><td>2.2</td><td>664</td><td>0.19</td><td>664±3.1799</td><td>42</td><td>3.14</td><td>0.191</td><td>52.356</td><td>10.8</td></tr>
<tr><td>35</td><td>2.5</td><td>632</td><td>0.35</td><td>632±5.490</td><td>39</td><td>3.31</td><td>0.181</td><td>55.249</td><td>8.4</td></tr>
<tr><td>40</td><td>2.8</td><td>616</td><td>0.38</td><td>616±5.7139</td><td>30</td><td>2.86</td><td>0.210</td><td>47.619</td><td>6.6</td></tr>
<tr><th colspan="10">B</th></tr>
<tr><th>Segment</th><th colspan="2">Flow rate ml.min^{-1}</th><th colspan="2">Intercept(a) mV</th><th colspan="2">Slope(b) mV/ mM</th><th colspan="2">correlation coefficient(r)</th><th>Angle ɵ</th></tr>
<tr><td>S_1</td><td colspan="2">0.9-1.3</td><td colspan="2">2668.31</td><td colspan="2">-1101.84</td><td colspan="2">-0.967</td><td>-89.948</td></tr>
<tr><td>S_2</td><td colspan="2">1.3-1.6</td><td colspan="2">2011.43</td><td colspan="2">-651.43</td><td colspan="2">-0.925</td><td>-89.912</td></tr>
<tr><td>S_3</td><td colspan="2">1.6-2.2</td><td colspan="2">1988.00</td><td colspan="2">-592.86</td><td colspan="2">-0.961</td><td>-89.903</td></tr>
<tr><td>S_4</td><td colspan="2">2.2-2.8</td><td colspan="2">837.33</td><td colspan="2">-80.00</td><td colspan="2">-0.982</td><td>-89.284</td></tr>
<tr><td colspan="10">ȲZi(mV):(S/N response of NAG-4SX3-3D Analyzer) in mV((S/N)-R.N.A), t0.025,2=4.303, SEM= Standard error of mean ΔtB(sec) :Base width of peak (sec), tsec : Departure time of sample segment out of injection valve reaching the flow cell, C :(Concentration), D.f : at the flow cell, a dilution factor.</td></tr>
</table>

3.5.2. Sample volume

Using the ideal settings found during earlier tests. As an analyte, Co^{+2} sample volume (S.V) effect (10 mM) was used. We chose the best sample volume for this study using a variety of Teflon tubes, ranging in length from 3.18 to 29.0 cm and having an inside diameter of 1 mm. The outcomes were summarized in Table 6A. It was seen from Figure 6 that the base width (Δ_{tB}) increased with a sample volume's length. This happens because the transport stream takes a long time to pass through the injection valve, which limits flow and increases the segment's dispersion of precipitate particles. Additionally, this causes an increase in the phenomenon of optical fiber at the convex part of the sample segment and the concave part at the end of the segment, which increases the light intensity that is applied to the particulate, increasing their agglomerates and density with an increasing precipitate segment. In this investigation, a compromise was established by selecting a sample volume of 120 µL as the most acceptable and practical. Based on the calculations for intercept (a), slope (b), correlation coefficient (r), and angle (Θ) (Table 6B and Figure 6), segment S3 (i.e., 80-228 µL) was selected as the chosen segment, and 120 µL within the chosen section included the optimal sample volume, which was going to be used in the subsequent experiments that were going to be done.

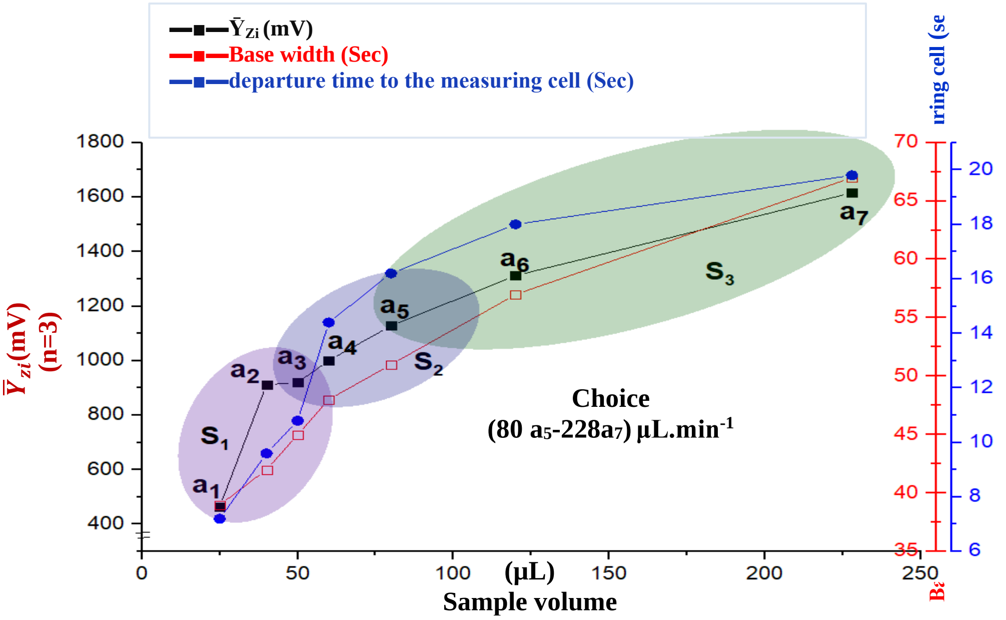

Figure 6: $\bar{Y}_{Z\,i}$ (mV) (S/N)-RNA and three data points as a single segment with the best option

Table 6A: Impact of S.V variation on precipitation of Co^{+2}, B: Using a segmentation pattern (a,b, r, and ϴ) of Co^{+2} (10mM)-$[Fe(CN)_6]^{-4}$ (5 mM)-HNO_3 (150 mM) system's at 1.6 mL/min (flowrate) for each line, best segment was chosen

A

Sample section length (cm) r= 0.5mm	**S.V µL**	**$\bar{Y}_{Zi}$(mV) (n:3)**	**%RSD σ_{n-1}(n;3)**	**CI at 0.05 $\bar{Y}_{Zi}$(mV)± t*$\sigma_{n-1}/\sqrt{3}$**	**Δt_BSec**	**V(mL) add**	**C (mM)**	**D.F**	**t_{sec}**
3.18	25	464	0.50	464±5.7388	39	2.105	0.119	84.034	7.2
5.10	40	912	0.27	912±6.161	42	2.280	0.175	57.143	9.6
6.37	50	920	0.17	920±3.9500	45	2.450	0.204	49.020	10.8
7.64	60	1000	0.18	1000±4.5463	48	2.620	0.229	43.667	14.4
10.20	80	1128	0.17	1128±4.9438	51	2.800	0.286	35	16.2
15.30	120	1312	0.18	1312±5.7636	57	3.160	0.380	25.315	18.0
29.00	228	1616	0.15	1616±6.2356	67	3.8013	0.599	16.719	19.8

B

Segment	**S.V µL**	**Intercept(a) mV**	**Slope(b) mV/ mM**	**correlation coefficient(r)**	**Angle ϴ**
$S_1(a_1-a_3)$	25-50	30.95	19.16	0.9236	87.012
$S_3(a_3-a_6)$	50-80	581.71	6.86	0.9983	81.700
$S_5(a_5-a_7)$	80-228	895.96	3.20	0.9930	72.628

$\bar{Y}$Zi(mV):(S/N response of NAG-4SX3-3D Analyzer) in mV((S/N)-R.N.A), t 0.025,2 = 4.303, SEM = Standard error of mean, ΔtB (sec): Base width of peak (sec), tse : Departure time of sample segment out of injection valve reaching the flow cell, C: Concentration, Df: Dilution factor at flow cell.

3.5.3. Reaction delay coil

Co^{+2} (10 mM) and $Ca_2[Fe(CN)_6]$ (5 mM) are mixed with HNO_3 (150 mM) and 120 µL of an injection sample. Both the carrier stream (Nitric acid 150 mM) and reagent stream flow at 1.6 mL.min^{-1} with variable coil volumes (0, 10, 20, 25, and 30 cm). The use of reaction coils will help to regulate and arrange the particulate in a regular order before reaching the laminar flow, avoiding the turbulent flow that will disturb the signal profile before entering the flow tube (Table 7A). Finally, a compromise between sensitivity and the use of delayed reaction coils revealed that there was no need to link the reaction coil to the manifold system. Due to the ideal manifold design used in this study endeavor, it will attain the high sensitivity that is mostly needed at this point. Based on the slope-intercept, correlation coefficient, and angle (Figure 7), segment S1 (i.e., 0-628 µL) was determined to be the ideal segment. We then conducted additional testing within the chosen section using the optimal delay response coil.

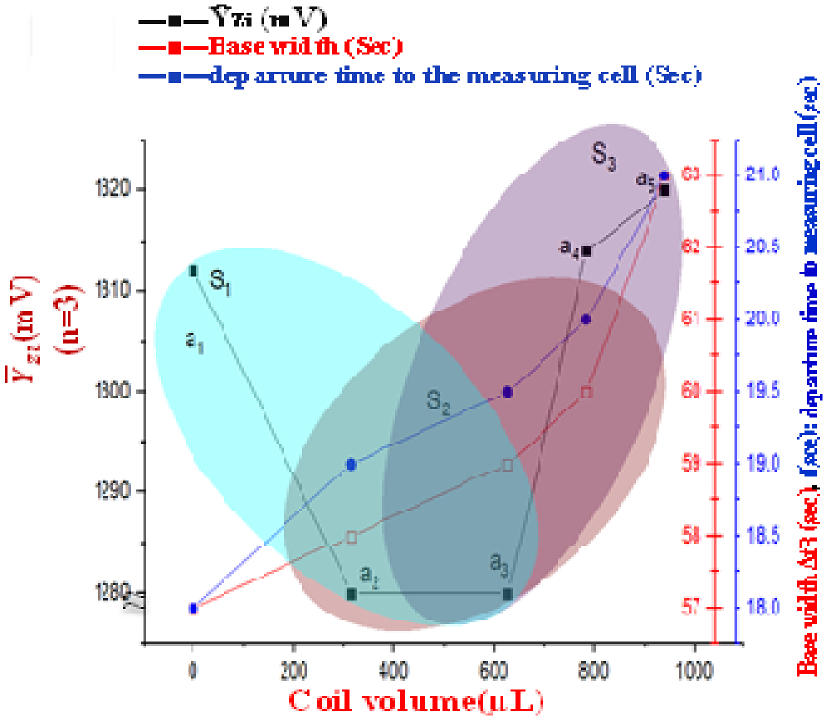

Figure 7: $\bar{Y}_{Z\,i}$ (mV) $\bar{Y}_{Z\,i}$ (mV) (S/N)-RNA and three data points as a single segment with the best option

Table 7A: Reaction coil length and volume effect on precipitation of Co^{+2}. **7B**: Using a segmentation pattern (a,b, r, and Ɵ) of Co^{+2} (10mM)-$[Fe(CN)_6]^{-4}$ (5 mM)-HNO_3 (150 mM), the system's flow rate was 1.6 mL/min for each line and 120 µL sample volume. The best segment was chosen

A

Coil length cm r = 1 mm	**Coil volume µL**	**$\bar{Y}_{Zi}$(mV) average (n=3)**	**RSD% σ_{n-1}(n=3)**	**Confidence interval at 0.05 $\bar{Y}_{Zi}$(mV)± t * $\sigma_{n-1}/\sqrt{3}$**	**Δt_B Sec**	**V_{add} (ml) at flow cell**	**C (mM)**	**D.F**	**t_{sec}**
Without	0	1312	0.15	1312±4.770	57	3.160	0.380	26.333	18.0
10	314	1280	0.16	1280±4.920	58	3.213	0.373	26.778	19.0
20	628	1280	0.18	1280±5.740	59	3.267	0.367	27.222	19.5
25	785	1312	0.11	1312±5.328	60	3.320	0.361	27.667	20.0
30	942	1320	0.09	1320±3.031	63	3.480	0.345	29.000	21.0

B

Segment	**Coil volume (µL)**	**Intercept(a) (mV)**	**Slope(b) (mV/ mM)**	**correlation coefficient (r)**	**Angle (Ɵ)**
$S_1(a_1-a_3)$	0-628	1306.66	-0.051	-0.8660	-2.917
$S_2(a_2-a_4)$	314-785	1257.14	-0.058	0.7560	3.333
$S_3(a_3-a_5)$	628-942	1204.00	0.127	0.9450	7.260

ȲZi(mV):(S/N) response of NAG-4SX3-3D Analyzer in mV((S/N)-R.N.A), t 0.025,2 = 4.303, SEM = Standard error of mean ΔtB (sec) : Base width of peak (sec), tsec: Departure time of sample segment out of injection valve reaching the flow tube, C: Concentration at flow cell, Df: Dilution factor at flow cell.

3.5.4. Y-Junction point pattern

For feasible products, mixing reactant reaction solutions that will lead to a reaction product (or products) is clearly important. This study utilized two sets of mixing points..

A. Intersection junction.
a) Two 2mm arms of the letter Y lading to a 4 mm tube diameter.
b) Two 4mm arms of the letter Y leading to a 6 mm tube diameter.
B. The length and diameter of the premix chamber determine its characteristics.
a) 12 mm in diameter and 14 mm in length; total volume: 1.85 μL.
b) 13 mm diameter with 14 mm length of total volume of 2.0 μL 14 mm.
c) 14 mm in diameter with a 14 mm length and a total volume of 2.15 μL.

The best place for the Y-junction to mix reactants and make particles precipitate in nitric acid medium was where the two 2 mm arms met. This was done with 12-56 μL, which is the perfect volume for the Y-junction (Table 8).

Table 8: A collection of data points has been gathered for the volume of the Y-junction and the premix chamber in the process of determining the concentration of Co(II) ion

Y-junction type(mm)		**Volume $\pi r^2 h$**	**$\bar{Y}_{Zi}$(mV) average (n=3)**	**t_{sec}**	**Volume mL**	**C (mM) DF**
					At the intersection	
Intersection junction point	2 mm (ID) (two inlet) 4 mm (thickness) (outlet)	12.56 μL	1312	17.0	1.027	1.169 8.556
	4 mm (ID)(two inlet) 6 mm (thickness) (outlet)	75.36 μL	952	19.2	1.144	1.048 9.533
Premix chamber	14 mm (ID) 12 mm (thickness)	1.85 mL	1312	21.0	1.240	0.968 10.333
	14mm (ID) 13 mm (thickness)	2.00 mL	1080	21.5	1.267	0.947 10.556
	14 mm (ID) 14 mm (thickness)	2.15 mL	816	21.7	1.277	0.939 10.644
t: Time (Sec) between the injection value and the junction point or premix chamber, C: Concentration before junction point or premix chamber, and DF: Dilution factor						

3.5.5. Variation of the energy transducer's response to Co^{+2} concentration

Utilizing the stated best practices for chemical and physical variables *via* the use of a manifold design system as shown in Figure 8A, the Co^{+2} solutions were generated in a range of concentrations (0.05-30 mM); this will serve as the x-axis (independent variable). We used the NAG-4S3X-3D analyzer to measure the degree of dilution of the incoming light. It offered (S/N) energy transducer responses as the y-axis (the dependent variable represented), as seen in Figure 8B, with the peak heights (analogue) of responses rising as the sample(conc) climbed. The scatterplot is ranging (0.05-30 mM), i.e., selection of all 27 points with a correlation coefficient of r = 0.9562 as shown in Table 9. The calibration range is explained as an increase in Co^{+2} concentration leading to an increase in precipitate particulates to 20 mM. Next, we observed a broadening of the peak height maximum, which corresponded to an increase in the number of precipitate particles present. Additionally, a rise in particle size reduces interstitial gaps and reflecting surfaces, slows down particle movement, and increases the amount of time particles spend in front of the detector, leading to a distorted response. Analytical range (dynamic range (D.R.)) extends from (0.05-25) mM (n = 24) with r = 0.9847; working range (W.R.) (0.05-21) mM (n = 21) with r = 0.9894; and linear range (linear dynamic range (L.D.R.)) (0.05-20) mM (n = 20) with r = 0.9893. When searching for better representation, a shorter range should be selected to improve the assessment of mathematical formulation. Table 9 tabulates all the collected data and includes the calibration region. These results include the correlation coefficient (r), the coefficient of determination

(r^2), the percentage capital R-squared (R^2), and the t-value for the calibration curve's linearity. The following linear equation, with r = 0.9893 and R^2% = 97.87, provides the most accurate description of the relationship between the concentration of Co^{+2} and the diminished intensity of incoming light..

$\hat{Y}_{Zi}$ (mV) = 129.204±74.652+97.862±7.132 [Co(II)] mM

The evaluation of the proposed technique for the identification of Co^{+2} was contrasted with the traditionally used method [25], namely the UV spectrophotometric method, which is based on measurements of absorbance at λ_{max} = 275 nm and 510 nm.

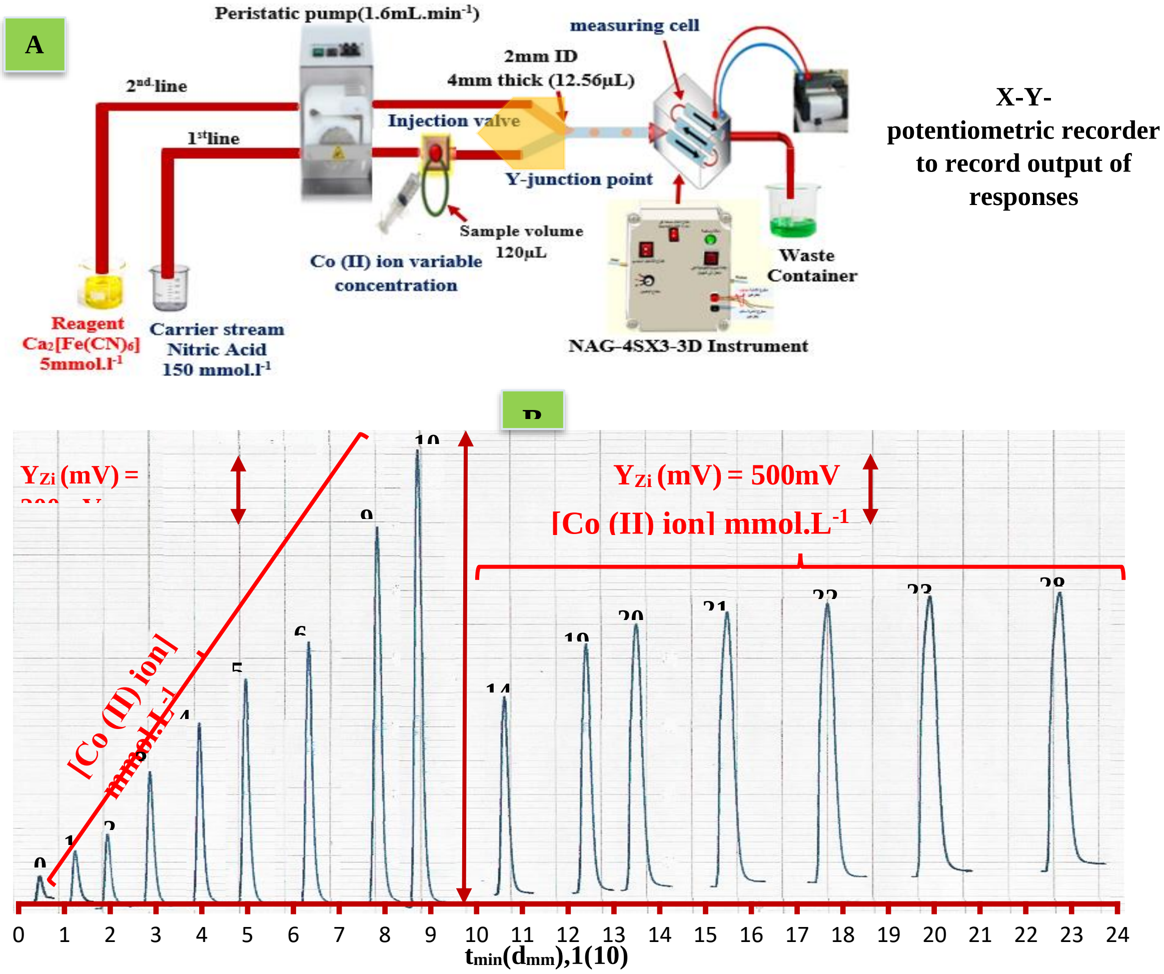

Figure 8A: Co^{+2} was determined using a flow gram system. **8B**: Several profiles against time and scanning speed for potentiometry (1 cm.min^{-1})

Table 9: Using the first degree equation of the form = a + b x under ideal circumstances, a summary of the findings of linear regression for the change of (S/N) energy transducer response with Co^{+2} concentration

Type of mode	**Range of $[Co^{2+}]$ mM-(n)**	**$\hat{Y}_{Z\,i}$=a ± S_a t+b(Δ y $_{/}$Δ$x_{mmol/L)}$ ± S_b t [Co (II)] mM At 95% confidence level for n-2**	**r, r^2, R^2%**	**t_{tab} at 95%, n-2**	**Calculated t-value t_{cal}=/r/√n-2 / √1-r^2**
Developed method using NAG – 4SX3 – 3D analyzer					
UV- Spectrophotometer at λ_{max}= $275_{nm.}$ and 510_{nm}					
inear range or linear dynamic	0.05-20(20)	129.204±74.652+97.863±7.132[Co (II)] mM	0.9893,0.9780, 97.80	2.101 << 28.819	
	0.01-5(22) 0.02-8(25)	0.1359±0.0384+0.2756±0.0169 [Co (II)] mM -0.0197±0.0149+0.2233±0.0043 [Co (II)] mM	0.9914,0.9828,98.28 0.9990,0.9980, 99.80	2.086<<33.848 2.069<< 105.907	
Working range or calibration range	0.05-21 (21)	139.581±75.419+95.815±6.737 [Co (II)] mM	0.9894,0.9780, 97.80	2.093 << 29.761	
	0.01-5.5(23) 0.02-9(26)	0.1435±0.0412+0.2672±0.0166 [Co (II)] mM 0.0332±0.0290+0.2147±0.0076[Co (II)] mM	0.9908,0.9817,98.17 0.9964,0.9929, 99.29	2.080<<33.563 2.064 << 57.814	
Dynamic range or analytical range	0.05-24 (24)	184.526±91.905+880121±6.690 [Co (II)] mM	0.9847,0.9697, 96.97	2.074<< 26.521	
	0.01-6(24) 0.02-10(27)	0.1543±0.0475+0.2564±0.0174 [Co (II)] mM 0.0534±0.0470+0.2030±0.0113 [Co (II)] mM	0.9884,0.9769,97.69 0.9911,0.9822, 98.22	2.074<<30.491 2.060 << 37.158	
Scatter plot	0.05-30(27)	283.422± 147.527+74.353±9.377 [Co (II)]mM	0.9562,0.9143, 91.43	2.060 << 16.333	
	0.01-7(25) 0.02-11(28)	0.1770±0.0656+0.2373±0.0217 [Co (II)] mM 0.0773±0.0642+0.1903±0.0140[Co (II)] mM	0.9781,0.9567,95.67 0.98390.9680, 96.80	2.069<<22.552 2.056 << 28.048	
n: no. of evaluations, ŶZi (mV); calculated responses (n = 3) in mV for the established approach combined with no unit for UV-spectrophotometry, r,r2,R2: explained variation as a percentage / total variation, ttab = t 0.05/2, n-2, and volume of measuring cell = 4 mL					

3.5.6. Limit of detection (LOD)

The numerical value of slope, stepwise dilution of the lowest concentration in the scatter plot, and linear equation were all employed to estimate the L.O.D. of the Co^{+2}[26]. All of these calculation values for detection limits, LOD for the conventional technique, and L.O.Q. for a 120 µL sample volume were summarized in Table 10.

Table 10: LOD of Co^{+2} using the ideal settings and a 120 µL injection sample; Co (II) (10mM)-$[Fe(CN)_6]^{-4}$(5 mM)- HNO_3 (150 mM) system

Based practically on the scatter plot's minimum concentration's progressive dilution		theoretically constructed using the slope's value. X = $3S_B$/slope	theoretically constructed using the linearity equation $\hat{Y} = Y_b + 3Sb$	Limit of quantitative (L.O. Q) $\hat{Y} = Y_b + 10S_b$
Recently developed technique (10 µmmo.L^{-1})	traditional technique (0.0009 mM at 275 and 510 nm)			
349.236 ng/sample	1.048 ng/sample	192.706 ng/ sample	38.041 µg/sample	0.127* 10^9ng/sample

3.5.7. Repeatability

Measurements of two concentrations of Co^{+2} are summed together in the measurement of precision attained during the whole assay procedure shown in Table 11. We conducted evaluations eight times for each sample. The results demonstrate that the relative standard deviation (RSD%) was less than 0.4%. A kind of response curve for the quantity measured.

Table 11: Repeatability of Co(II) ions at optimum parameters with a 120 µL sample volume

Co(II) ion (mM)	**$\bar{Y}_{Zi}$ (mV) average of responses (n = 8)**	**RSD% σ_{n-1}(n = 3) σ_{n-1}**	**Confidence interval at 95% $\bar{Y}_{zi}$ (mV)± $t_{0.025}\sigma_{n-1}/\sqrt{n}$**
5	664	0.35 2.32	664± 1.940
10	1312	0.15 1.92	1312± 1.605
$t_{0.025,7}$=2.365, n = number of injections			

3.5.8. Analyzing Co^{+2} in alloys using a home-made NAG-4SX3-3D device

The established method was used for the determination of Co(II) ion in two different kinds of Co(II) ion alloys from two well-known alloy manufacturers (high purity iron (B.C.S.No.260/2)) (0.009%, i.e., 9 mg in 100g) and (high purity iron (B.C.S.No.149/2)) (0.012%, i.e., 12 mg in 100g) using the NAG-4S3X-3D analyzer and compared with the classical spectrophotometric method against the measurement of λ_{max} at 510 nm [25]. The standard addition method was applied by preparing a series of solutions from each alloy: the first alloy (0.15 mM - 0.9 mg of active ingredient in 100 mL) and the second alloy (0.203 mM - 1.2 mg of active ingredient in 100 mL) by transferring 0.8 mL of the first alloy and 5.91 mL of the second alloy to each of the five volumetric flasks (10 mL), followed by the addition of gradual volumes of 50 mM standard Co^{+2} (0, 0.2, 0.4, 0.6, and 0.8 mL), which are equivalent to 0, 1, 2, 3, and 4 mM for both the NAG-4SX3-3D (NAG) analyzer and the classical UV-spectrophotometric method. Figure 10 shows the response profile for this study. The findings of two methods are summarized in Table 12, which also includes a t-test for comparison between the two routes, efficiency of determination, and practical amount of active component at a 95% confidence level [26, 27].

Individual t-test: A comparison between a freshly discovered method and an officially indicated value (μ_0 = ((H.P.I.) (B.C.S.No.260/2)) (0.009%, i.e., 0.9 mg in 100 g), ((H.P.I.) B.C.S.No.149/2)) (0.012%, i.e., 12 mg in 100 g), as shown in Table 11 by calculated $t_{.cal}$ of an individual company, a hypothesis can be calculated as follows:

H_o (null hypothesis): for sample no. 1: $\mu_0 = \overline{W}_1$ for UK
for sample no. 2: $\mu_0 = \overline{W}_2$ for UK

i.e., there is no significant difference between the means of particle content for four different companies ($\overline{W}_i$) and the quoted value (μ_0 = 0.9 or 1.2 mg) against

H_1 (alternative hypothesis): $\mu_0 \neq \overline{W}_i$ for two different samples

Specifically, the stated value and mean of practical content for two independent samples differ significantly from each other.

According to the findings, there is no significant difference between the quoted value (0.9 mg or 1.2 mg) and the estimated t-value at the 95% confidence level of the samples, which suggests, i.e., t_{tab}> tcal.

Paired t-test: It was conducted for comparison between the developed method of analysis (i.e., using the NAG-4SX3-3D analyzer) and classical methods (spectrophotometric and reference official method) of two samples from two different companies. Taking into consideration a neglected individual difference between one manufacturer and another. The calculation's tcal is 0.916 < 12.706. At a 95% confidence level, We conclude that there is no discernible difference between the two procedures, and we accept H_0 against H_1.

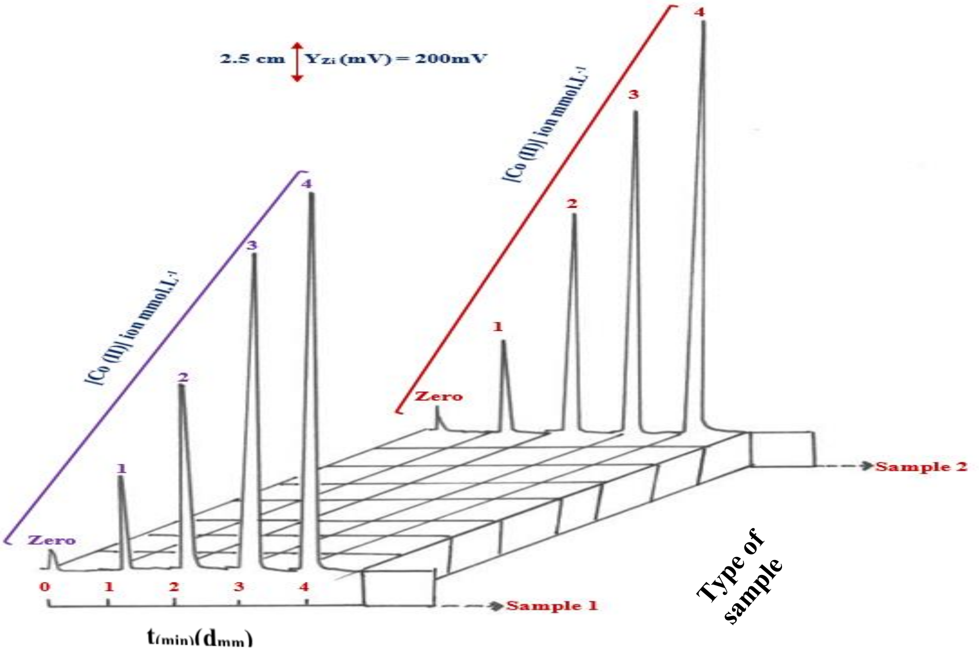

Figure 10: Profile - time for the standard addition method using two different samples:
Sample 1: (H.P.I.) (B.C.S.No.260/2)
Sample 2: (H.P.I.) (B.C.S.No.149/2)

Table 12: Results for efficiency and practical content (Rec%) to determine Co^{+2} in two samples of alloys and t-tests for contrasting two approaches are summarized

Type of method					
new method					
UV- Spectrophotometric at λ $_{max}$= 510nm.					
Co(II) (mM)					
0		**0.2ml**	**0.4ml**	**0.6ml**	**0.8ml**
0		**1**	**2**	**3**	**4**
Type of alloy	**Weight of Co(II) ion in 100gm alloy**		**Weight of alloy in 10 gm (mg)**		**[Co(II)] mM of 10gm alloy**
(High purity iron (B.C.S.No.260/2)) 0.009%	**9**		**0.9**		**0.1527**
New method response	**40**	**230**	**440**	**728**	**880**
UV- Spectrophotometric absorbance	**0.06**	**0.32**	**0.63**	**0.89**	**1.26**
Equation of standard addition at 95% confidence level for n-2,r,r^2andR^2%					
New method equation	**$\hat{Y}_i$(mV)=a±s_at+b±s_bt [Co(II)]mM, r,r^2andR^2% =28.0±84.0770+217.80±34.3242 [Co(II)]mM,0.9963,0.9927,99.27**				
UV- Spectrophotometric equation	**$\hat{Y}_i$=a±s_at+b±s_bt [Co(II)]mM r,r^2andR^2% =0.038±0.0827+0.297±0.0337 [Co(II)]Mm,0.9981,0.9962,99.62**				
(high purity iron (B.C.S.No.149/2)) 0.012%	**1.2**		**12**		**0.203**
New method response	**54**	**216**	**492**	**736**	**950**
UV- Spectrophotometric	**0.05**	**0.36**	**0.72**	**1.08**	**1.39**

absorbance					
Equation of standard addition at 95% confidence level for n-2,r,r^2andR^2%					
New method equation	**$\hat{Y}_i(mV)=a\pm s_a t+b\pm s_b t$ [Co(II)]mM, r,r^2andR^2% =27.2±74.7169+231.2±30.5030 [Co(II)]mM,0.9974,0.9949,99.49**				
UV- Spectrophotometric equation	**$\hat{Y}_i=a\pm s_a t+b\pm s_b t$[Co(II)]mM r,$r^2andR^2$% =0.04±0.0449+0.34±0.0185 [Co(II)]mM,0.9996,0.9991,99.91**				
Efficiency of determination Rec.%					
(B.C.S.No.260/2)) 0.009%	**105.23**				
	104.72				
(B.C.S.No.149/2)) 0.012%	**97.76**				
	97.76				
Individual t-test between claimed value & practical value= ($\bar{W}_{i(mg)}$-) $\sqrt{n}$ /σ_{n-1},σ_{n-1}					
2.459< 4.303 σ_{n-1}=0.331					
/1.652/<4.303 σ_{n-1}=0.238					
Paired t –test Compared between two methods **$t_{cal}=\bar{w}d\sqrt{n}/\sigma^*_{n-1}$, t_{tab} at 95%confidence level (n-1)** **Newly developed methodology and quoted value (reference method)** **$\bar{W}d$ = 0.0215** **σ^*_{n-1}= 0.0332** **0.916< 12.706**					
µ: Claim value (9mg/100 g and 12 mg/100g), $\bar{w}i$: Weight practically in mg, $\bar{W}d$: The weighted average of the differences σ_{n-1}:standard deviation of different(paired t-test), n:(no. of sample) = 2, $t_{tab}=t_{0.05/2\ ,n-1}=t_{0.025,3}$ = 12.706 (for individual t-test & paired t-test), classical method: UV-Spectrophotometric method					

.

4. Conclusion

The procedure exhibits enhanced sensitivity, reduced reagent consumption, and superior outcomes compared to the conventional reference method utilizing 10 mm irradiation. Traditional methods of finding cobalt (II) ions were not as effective as the one that was proposed. The equipment and chemicals needed for the suggested method are also much more affordable. The NAG-4SX3-3D analyzer provided a finding that was both more accurate and quicker within the context of this research. The repeat's RSD% (n = 13), which is substantially lower than 0.36%, is evidence that the suggested approach is accurate enough. This technique also has the advantage of obtaining high sensitivity without the need for temperature or the extraction process, which is helpful for detecting the cobalt (II) ion. This allows you to save a ton of time.

Acknowledgments

My sincere appreciation goes out to Prof. Issam M.A. Shakir for his invaluable counsel, insightful observations, and encouragement.

References

[1] I. Pronina, E. Mochalova, Y. A. Efimova, and P. Postnikov, "Biological functions of cobalt and its toxicology and detection in anti-doping control", *Fine Chemical Technologies*, vol. 16, no. 4, pp. 318-336, 2021.

[2] S. Khalil and M. El-Sharnouby, "Construction of a highly selective membrane sensor for the determination of cobalt (II) ions", *Chemosensors*, vol. 9, no. 5, p. 86, 202.

[3] M. Jamaluddin Ahmed and K. Jakir Hossan, "A rapid spectrophotometric method for the determination of cobalt in industrial, environmental, biological, pharmaceutical and soil samples using bis (5-bromosalicylaldehyde) orthophenylenediamine", *Journal of the Iranian*

Chemical Society, vol. 5, no. 4, pp. 677-688, 2008.

[4] S. Li, J. Li, X. Ma, C. Pang, G. Yin, and J. Luo, "Molecularly imprinted electroluminescence switch sensor with a dual recognition effect for determination of ultra-trace levels of cobalt (II)", *Biosens Bioelectron,* vol. 139, Article no. 111321, 2019.

[5] V. A. Pedrosa and M. Bertotti, "Electrochemical behavior of thin ruthenium-modified cobalt-hexacyanoferrate films immobilized on self assembled monolayer gold electrodes", *International Journal of Electrochemical Science,* vol. 2, pp. 113-122, 2007.

[6] M. A Hamood and M. A Abed, "Oxidation study of cobalt-base super alloys at high temperatures in molten salt of Na_2SO_4", *Rafidain Journal of Science,* vol. 23, no. 7, pp. 127-136, 2012.

[7] R. Ali, P. Song, M. Khan, T. Huang, S. Ali, S. H. Sha, J. Lu, Z. Ul Wahab, and S. Pervaiz, "The effect of pre-oxidation on the hot corrosion behavior of CoNiCrAlHf alloy in Na_2SO_4 environment at elevated temperature", *Applied Physics A,* vol. 128, no. 9, p. 756, 2022.

[8] M. R. Jamali, P. Khodayar, and R. Rahnama, "Ultrasound-assisted dispersive magnetic solid phase extraction using toner powder for the separation and preconcentration of cobalt in water and food samples and determination by flame atomic absorption spectrometer", *Journal of Dispersion Science and Technology,* pp. 1-9, 2023.

[9] M. Q. Al-Abachi, S. S. Abed, and N. A. Al-Najjar, "A New Chromogenic Reagent for Determination of Copper (II) in Water Samples Using Flow injection-Technique," *Iraqi Journal of Science,* vol. 58, no. 1B, pp. 201-210, 2017.

[10] W. A. Al-Uzri, M. Jamal, and H. Hadi, "Colorimetric Determination of Salbutamol Sulfate using Spectrophotometry-Continuous Flow Injection Technique in Pure and Pharmaceutical Forms," *Iraqi Journal of Pharmaceutical Sciences (P-ISSN 1683-3597 E-ISSN 2521-3512),* vol. 32, no. 1, pp. 45-52, 2023.

[11] M. Q. Al-Abachi, S. S. Abed, and M. H. A. Alamri, "Charge transfer spectrophotometric determination of metronidazole in pharmaceutical formulations by normal and reverse flow injection analysis coupled with solid-phase reactor containing immobilized FePO4," *Iraqi Journal of Science,* pp. 1541-1554, 2020.

[12] J. N. Jeber,Nagham S.T "A turbidimetric method for the quantitative determination of cyproheptadine hydrochloride in tablets using an optoelectronic detector based on the LEDs array", *International Journal of Pharmaceutical Research,* vol. 12, no. 4, pp. 2911-2924, 2020.

[13] C. Zhao, X. Li, C. Cheng, and Y. Yang, "Green and microwave-assisted synthesis of carbon dots and application for visual detection of cobalt(II) ions and pH sensing", *Microchemical Journal,* vol. 147, pp. 183-190, 2019.

[14] S. H. Lee *et al.*, "Oxidation state and surface reconstruction of Cu under CO2 reduction conditions from in situ X-ray characterization," *Journal of the American Chemical Society,* vol. 143, no. 2, pp. 588-592, Jan 20 2020.

[15] V. Zaichick, "A systematic review of the strontium content of the normal human prostate gland," *Jour Med Resh and Health Sci,* vol. 4, no. 5, pp. 1257-1269, 2021.

[16] S. Capiau *et al.*, "Development, validation and application of an inductively coupled plasma–mass spectrometry method to determine cobalt in metal-on-metal prosthesis patients using volumetric absorptive microsampling," *Talanta,* vol. 208, p. 120055, Feb 1 2020.

[17] N. E. Karlıdağ, R. Demirel, H. Serbest, F. Turak, and S. Bakırdere, "Determination of cobalt in chamomile tea samples at trace levels by flame atomic absorption spectrophotometry after poly (vinyl alcohol)-magnetic hydrogel based dispersive solid phase extraction", *Analytical Methods,* vol. 15, no. 1, pp. 56-62, 2023.

[18] W. Zeng, J. Hu, H. Chen, Z. Zou, X. Hou, and X. Jiang, "Cobalt ion-enhanced photochemical vapor generation in a mixed acid medium for sensitive detection of tellurium (IV) by atomic fluorescence spectrometry," *Journal of Analytical Atomic Spectrometry,* vol. 35, no. 7, pp. 1405-1411, 2020.

[19] Z. F. H. I. M. A. Shakir, "Chemiluminometric-CFIA for the determination of cobalt(ll) ion in commercial cobalt-molybdenum catalyst (K F124-3E) used in desulphurization processes of petroleum products via multi gel beads reactor", *Iraqi Journal of Science,* vol. 56, no. 1A, pp. 38-52, 2015.

[20] I. M. A. Shakir and Z. F. Hassan, "Novel chemilumino-fluorometric method for the determination of Co(II) ion in CoMo catalyst type (KF124-3E) based on the in situ irradiation of released chemiluminescence from poly acrylic acid gel beads saturated with luminol to fluorescein molecule using continues flow injection analysis in a specially designed cell", *International Journal of Research in Pharmacy and Chemistry,* vol. 5, no. 1 pp. 1-9, 2015.

[21] Z.-G. Wang *et al.*, "A highly selective colorimetric and fluorescent probe for quantitative detection of Cu2+/Co2+: The unique ON-OFF-ON fluorimetric detection strategy and applications in living cells/zebrafish," *Spectrochimica Acta Part A: Molecular and Biomolecular Spectroscopy*, vol. 228, p. 117763, 2020.

[22] I. A. Darwish, Z. Wang, R. J. Darling, and N. Z. Alzoman, "Development of two highly sensitive and selective sensor-assisted fluorescence immunoassays for trace determination of copper residues in food samples," *RSC Adv,* vol. 13, no. 42, pp. 29195-29205, Oct 4 2023.

[23] B. S. Mohammed and N. S. Turkey, "New homemade NAG-4SX3-3D analyzer for quantification of cyproheptadine hydrochloride by its precipitating with calcium hexacyanoferrate", *Chemical Papers,* vol. 78, pp. 1277-1290, 2023.

[24] A. I. Vogel, *A text-book of macro and semimicro qualitative inorganic analysis*. London Longmans,1954,p.654.[Online].Available:http://117.239.25.194:7000/jspui/bitstream/123456789/694/1/PRILIMINERY%20AND%20CONTENTS.pdf

[25] R. Singh *et al.*, "Colorimetric sensing approaches based on silver nanoparticles aggregation for determination of toxic metal ions in water sample: a review," *International Journal of Environmental Analytical Chemistry,* vol. 103, no. 6, pp. 1361-1376, 2023.

[26] J. Miller and J. C. Miller, "*Statistics and chemometrics for analytical chemistry*", Pearson education, 2018.

[27] A. Adeniran, J. Olilima, and R. Akano, "Analysis of Variance: The Fundamental Concepts and Application with R", *International Journal of Multidisciplinary and Current Research,* vol. 9, no. 10, pp. 2408-2422, 2021.